Journal of Applied Electrochemistry **33**: 1223–1231, 2003.

Effect of resistivity on the corrosion mechanism of mild steel in sodium sulfate solutions

S. ARZOLA[1], M.E. PALOMAR-PARDAVÉ[2] and J. GENESCA[1,*]
[1]*Departamento Ingeniería Metalúrgica, Facultad Química, UNAM, Ciudad Universitaria, 04510 México DF, Mexico*
[2]*Area Ciencia de Materiales, Universidad Autónoma Metropolitana-Azcapotzalco, 02200 México DF, Mexico*
*(*author for correspondence, e-mail: genesca@servidor.unam.mx)*

Received 12 June 2002; accepted in revised form 29 July 2003

Key words: corrosion mechanism, EIS, mild steel, resistivity, sulfate ions

Abstract

Electrochemical impedance spectroscopy (EIS) was used to study the corrosion behavior of mild steel samples immersed in 1, 0.1, 0.01 and 0.001% Na_2SO_4 aqueous solutions at room temperature in order to analyze the corrosion mechanism and obtain representative values of corrosion rates in environments with different resistivity. The EIS technique was used to measure corrosion current densities in 1 to 0.01% Na_2SO_4 solutions, and the measurement corresponding to 0.001% concentration gave a scattered Nyquist plot, whereas in the Bode representation a response associated with solution resistance was obtained. Other electrochemical techniques such as linear polarization resistance, LPR, Tafel extrapolation method and electrochemical noise (EN) were used in order to compare the results obtained by EIS. The 'charge-transfer resistance' (R_{ct}) parameters obtained in the EIS technique agree well with the corresponding values of 'polarization resistance' (R_p) values obtained by the LPR technique, whereas the 'electrochemical noise resistance' (R_n) parameters obtained by the EN technique gave the highest values for all concentrations. These parameters generally tended to increase as the concentration of the solution decreased.

1. Introduction

The electrical resistivity of a soil is probably the most commonly used criterion of corrosivity because it is easy to measure. The resistivity of a soil depends on its chemical content, moisture content and temperature. Low-resistivity soils, for instance, generally contain high concentrations of soluble salts. The presence of anions in the salt degrades protective oxide films on steel, accelerating the rate of the electrochemical reactions at the metal surface.

Since macrocells are responsible for many of the instances of severe corrosion of underground structures, we would expect a correlation to exist between soil moisture content and underground corrosion. Such correlations are found in the literature. For example, Booth et al. [1] found that only resistivity and redox potential were better predictors of corrosiveness than moisture content. Data showing the effect of salt content (chlorides and sulfates) on the resistivity of single salt solutions are also found [2]. These data show a systematic trend of decreasing resistivity with an increasing concentration profile for $CaSO_4$ (as sulfate) and NaCl (as chloride) solutions.

A wide variety of soluble salts are typically found in soils. In fact two soils having the same resistivity may have significantly different corrosion characteristics, depending on the specific ions available. The major factors that accelerate corrosion are chlorides, sulfates, and the soil acidity (pH). Table 1 correlates the effect of sulfates and pH on the corrosion of buried steel or concrete structures.

In many areas soils encountered along a pipeline route will be approximately neutral, pH 7 [3]. Mild steel is widely used in pipes buried in soil. The corrosion of such metallic materials leads to numerous problems concerning, for example, water supply systems and soil pollution by ferric ions.

The corrosion of mild steel in agricultural irrigation waters, in fact has both economic and environmental consequences. Laboratory investigations are highly important but require knowledge of the physical and chemical properties of the soil, which can be affected by many factors, particularly by changes in the nature of soil.

Actually, steel in deareated, dry soil should not corrode at all, but must soils are not dry. Soil resistivities are an indication that moisture and dissolved salts are present, and the corrosivity of soil is almost proportional to the decrease in resistivity. Table 2 shows the relation of soil resistivity to corrosion rate of steel in soils based on 12-year tests of buried specimens by the U.S. Bureau of Standards [4].

Table 1. Effect of sulfates and pH on corrosion of buried steel pipelines

Concentration of sulfate /ppm	Degree of corrosivity	pH	Degree of corrosivity
⩾10,000	Severe	⩽5.5	Severe
1500–10,000	Considerable	5.5–6.5	Moderate
150–1500	Positive	6.5–7.5	Neutral
0–150	Negligible	⩾7.5	None (alkaline)

Table 2. Corrosion of steel in soil (Romanoff [4])

	Corrosion /mpy	Type	Soil resistivities /Ω cm
Average of 44 soils	61	Moderately corrosive	1000–2000
Tidal marsh	100	Corrosive	500–1000
California clay	137	Very corrosive	Below 500
Sandy loan (New England)	21	Mildly corrosive	2000–10,000
Desert sand (Arizona)	5	Noncorrosive	Above 10,000

As an initial approach and in order to study the corrosion of mild steel in electrolytes (soils) of different resistivity, Na_2SO_4 solutions of different concentration were employed to simulate them. It can be noted that sulfate ions are stable in water over a wide range of pH (≥2). This work also studies the extent to which the techniques 'linear polarization resistance', LPR, 'tafel extrapolation method', 'electrochemical impedance spectroscopy', EIS, and 'electrochemical noise', EN, can be correlated in order to obtain representative values of the corrosion rate in an environment of changing resistivity.

2. Experimental

The measurements were carried out on a solution of sodium sulfate, Na_2SO_4, of different concentrations, as shown in Table 3. For each concentration five measurements were taken, all at room temperature, and with atmospheric pressure and no oxygen control, thus allowing the atmospheric oxygen to dissolve freely in the solution in order to simulate natural conditions.

All the samples were cut from the same AISI 1020 mild steel rod (0.65 cm diameter), whose chemical composition is shown in Table 4.

Table 4. Typical chemical analysis of AISI 1020 mild steel

Chemical element	C	Mn	Si	P	S
%	0.18–0.23	0.30–0.60	0.25	0.04 max.	0.05 max.

Each sample used for electrochemical measurements had a total length of approximately 3 cm. The cut samples were first abraded with 120 commercial SiC grit paper, ending with 600 commercial SiC grit paper and later mechanically polished with 0.3 μm alumina to obtain a mirror-like finish. To avoid oxidation each sample was rinsed, first with tap water, secondly with distilled water and afterwards degreased in acetone and kept in a dessicator until use.

Thus prepared, the samples used for electrochemical impedance measurements were mounted in an epoxy resin, leaving a surface of 0.332 cm^2.

The experimental set-up used for EIS was a two-working electrode system. The main electronic equipment used was a Potentiostat/Galvanostat (Gamry model PC3) linked to a PC and a lock-in amplifier (Stanford Research System model SR810 DSP) controlled by the software CMS100, also from Gamry. The procedure employed was as follows: the mounted samples, having been immersed in the solution for 30 min, the impedance was measured from an initial frequency of 100 kHz to a final frequency of 50 mHz, a sufficiently small amplitude of 10 mV (rms) from the E_{corr} being used. The measurement was repeated daily during a 7-day period. The corresponding equivalent circuit, as well as the value of each of its elements, was derived using Thales fitting program from BAS.

The experimental arrangement used for LPR measurements was a three-electrode system. The electronic equipment used was a Potentiostat/Galvanostat (EGG model 273) linked to a PC and controlled by the software SoftcorrII M352. The procedure used was the following: after 30 min the corrosion potential was measured against a Hg/Hg_2SO_4 saturated reference electrode, then an overpotential of −20 mV was applied to the specimen, allowing the current to stabilize for 30 s. Afterwards the potential was swept at a scan rate of 0.16 mV s^{-1} up to an overpotential of +20 mV. The values of potential and current were sampled and stored by a PC every 1.641 s.

For ENM two identical working electrodes with a reference-electrode system (Hg/Hg_2SO_4) were used. The electronic equipment was the same as previously used

Table 3. pH and resistivity values of the Na_2SO_4 solutions as a function of its concentration

Solution Na_2SO_4	0% wt	0.001% wt	0.01% wt	0.1% wt	1% wt
Solution Na_2SO_4	0 ppm	10 ppm	100 ppm	1000 ppm	10,000 ppm
pH at 22 °C	6.96	6.86	6.77	6.76	6.64
ρ/Ω cm at 22 °C	212,765	93,458	11,236	1248	156
Type[a]	Noncorrosive	Noncorrosive	Mildly corrosive	Moderately corrosive	Very corrosive

[a] As predicted by Table 2.

for EIS measurements, with software CMS100. The procedure employed was as follows: two identical samples were immersed in the solution and connected via a potentiostat working as a zero resistance ammeter (ZRA). The circulating current between these identical samples and the potential of the couple against a Hg/Hg_2SO_4 of one sample were measured 30 min after the immersion. The measurement of these parameters was taken by a PC every 1.14 s, taking a total of 2058 readings. No filtering of the sampled data was used.

3. Results and discussion

To determine the stability of soluble species formed as a result of corrosion of mild steel in Na_2SO_4 solutions, a thermodynamic study was carried out on the basis of the predominance-zone diagrams, PZD, according to the model proposed by Rojas et al. [5], which is an alternative approach for establishing the predominance zones for chemical species in a single state. The diagram for the system Fe(II)–SO_4^{2-}–H_2O has been calculated (Appendix 1) and is shown in Figure 1a. The construction of Figure 1a is presented in the appendix. At the pH value of the Na_2SO_4 solutions, it is possible to obtain the PZD of Fe(II) species at pH = 7 (Figure 1b). This diagram is a slice cut from Figure 1 at pH = 7.

It is clear that, thermodynamically, mild steel corrosion in sulfate media proceeds by means of two different reactions, depending on the sulfate concentration:

if log $[SO_4^{2-}] < -2.25$, the thermodynamically favored corrosion process is

$$Fe_{(s)} \Leftrightarrow Fe^{2+}_{(aq)} + 2e \quad (1)$$

whereas if log $[SO_4^{2-}] > -2.25$, mild steel corrosion in Na_2SO_4 aqueous media will proceed according to

$$SO^{2-}_{4(aq)} + Fe_{(s)} \Leftrightarrow FeSO_{4(aq)} + 2e \quad (2)$$

The corrosion rate of mild steel as a function of sulfate concentration is shown in Figure 2. Assuming that the corrosion mechanism is controlled by activation (the rates of the electrochemical processes are controlled by the charge-transfer across the metal solution interface) as the Tafel diagrams suggest, sulfate can act as a depolarization agent of reaction (1), thus increasing the corrosion rate when $[SO_4^{2-}] > 0.1\%$, which is in good agreement with the PZD diagrams. It is clear that when the predominant species is $FeSO_4$, the corrosion rate increases significantly. The corrosion rate values obtained in Na_2SO_4 solutions are obviously lower than those obtained in soil (Table 2) because of the absence of Cl^-, among other reasons.

The morphology of the corrosion attack occurring on the surface of the mild steel after a 7-day exposure can be regarded as partially uniform. This attack started in isolated locations and spread laterally without developing any pits. Other authors, for example Thomas et al. [6], found that the corrosion process is uniform and the formation of a $FeSO_4$ ion pair complex is found in the presence of SO_4^{2-} ions only. As pointed out by Gui and Devine [7], the effect of SO_4^{2-} on the rate of oxidation of iron in mildly alkaline solutions results from its ability to form soluble complexes with either Fe^{2+} or Fe^{3+}.

The cyclic voltammogram of iron in these solutions suggests that dissolution of the metal is the major anodic process [8]. Florianovich et al. [9] found that sulfate ions

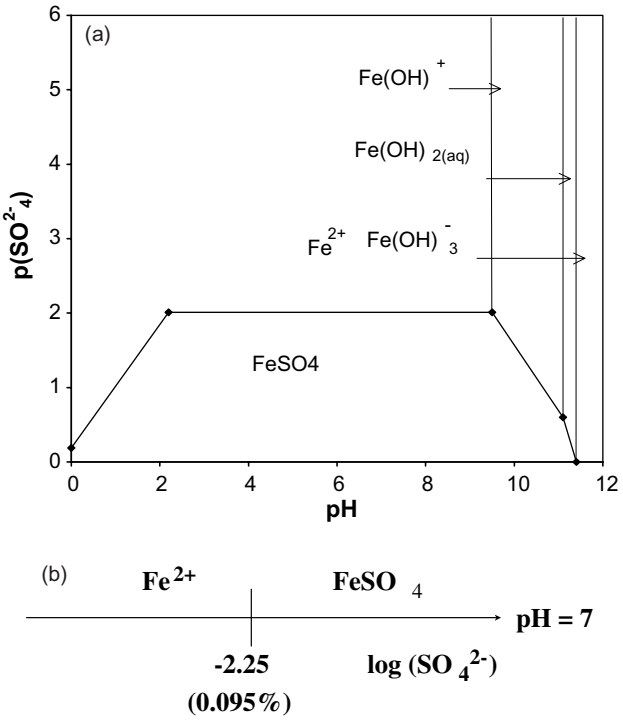

Fig. 1. (a) Two-dimensional PZD of Fe(II) species. (b) One-dimension PZD for the system Fe–H_2O–SO_2^{-4}.

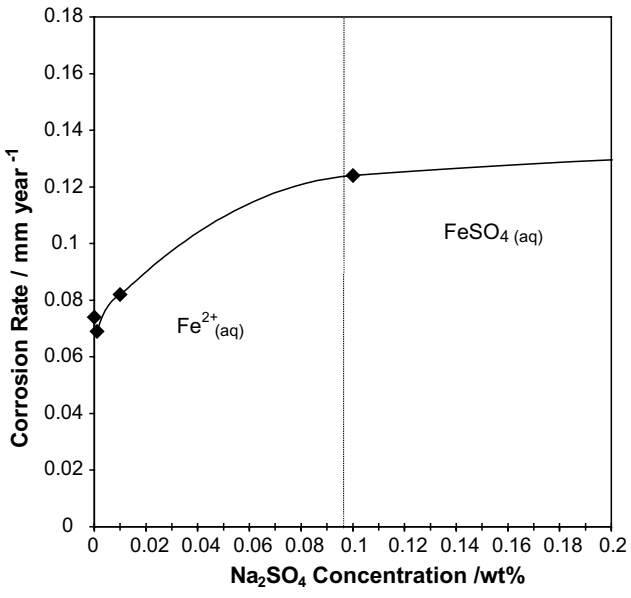

Fig. 2. Corrosion rate of AISI 1020 mild steel as a function of Na_2SO_4 concentration.

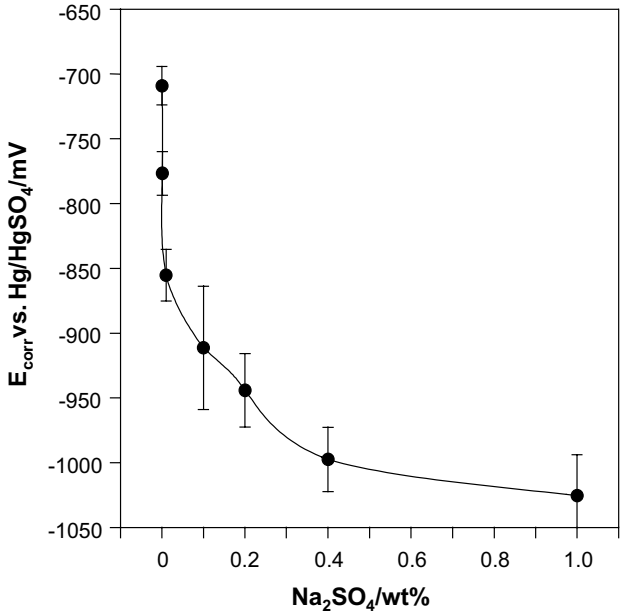

Fig. 3. Corrosion potential, E_{corr}, of AISI 1020 mild steel as a function of Na_2SO_4 concentration.

accelerate the active dissolution of iron, and other workers [10] concluded that films formed in sulfate solutions (pH 7) result from supersaturated solutions of iron salts, most probably of iron hydroxysulfate. This implies that iron dissolves in sulfate solutions at a high rate, creating a supersaturated solution and allowing precipitation of a film. These films were found [10] to be non-protective.

Corrosion potential, E_{corr}, as a function of Na_2SO_4 concentration is shown in Figure 3. The potentials measured at the moment of immersion quickly change towards more negative values, thus indicating the instability of the air-formed oxide in SO_4^{2-} solutions. Potential decreases from approximately −700 mV for 0% to −1000 mV (vs Hg/Hg_2SO_4) when the sodium sulfate concentration is 1%. This tendency (shift) to more negative potential values and the fact that the corrosion rate increases when the sodium sulfate concentration is higher (Figure 2) can be interpreted for a corrosion process controlled by a charge-transfer mechanism as a depolarization of the anodic reaction, which agrees with the mechanism previously proposed, according to the PZD diagram and thermodynamic considerations.

Under the study conditions evaluated here, oxygen reduction is the prevailing cathodic reaction, because all experiments were conducted under no-oxygen control condition. At pH ≈ 7 the oxygen reduction is expressed by the equilibrium:

$$O_2 + 2H_2O + 4e^- \leftrightarrow 4OH^-$$

In the other hand, the 'air-formed film' may not be stable under the studied conditions. After polishing, the surface of the steel was in contact with the air and an

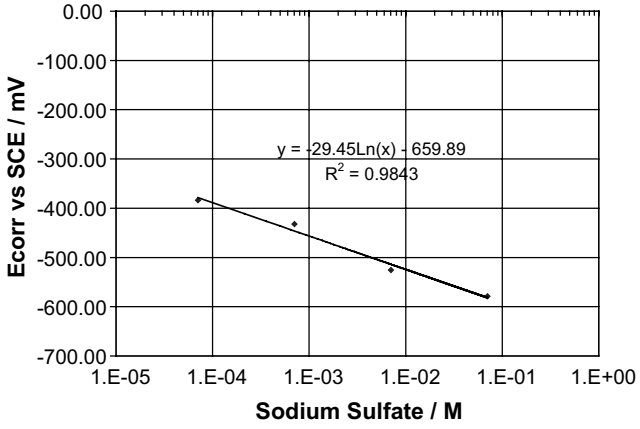

Fig. 4. Variation with addition of sodium sulfate of steady-state potential of steel electrodes in aerated distilled water.

'air-formed film', is present. However, as soon as the steel makes contact with the solution this film is dissolved. This is demonstrated by the open circuit potential values shown in Figure 3.

The way in which the final steady-state potentials of the steel electrode change with the molar concentration of the SO_4^{2-} ions is of interest. The curve in Figure 4 is a plot of these potentials as a function of the logarithm of the molar concentrations of the aggressive ion. The relation is linear and satisfies the equation $E_{corr} = -a - b\log[Na_2SO_4]$

$$E_{corr} = -659.9 - 29.45\ln[Na_2SO_4] \quad (3)$$

The value of constant a, i.e. the potential that would be measured in 1 M Na_2SO_4 solution, is obtained by extrapolation of the line and amounts to −659.9 V (SCE). Similar values were obtained for the same system by Abd El Kader et al. [11]. The aggressivity of the sulfate ions is, however, more pronounced in more dilute solutions, in which both the measured potentials and their rate of change with concentration (i.e. the value of coefficient b) are lower than they are in chloride solutions [11]. The slope of the line in Figure 4 is only 29.45 mV (ln concentration unit)$^{-1}$.

Equation 3 extends over four orders of magnitude of concentration and fulfills Brasher's theory [12] on the role of anions in promoting or inhibiting corrosion. According to this theory, all anions are corrosive when present in dilute solutions; however, they become inhibitive at sufficiently high concentrations. The concentration at which an anion changes its character depends on its nature. In the domain of corrosion promotion the steady-state potentials follow Equation 3. As a conclusion, the sulfate ion within the concentration range studied acts aggressively towards mild steel in aerated solutions.

3.1. *EIS analysis*

A better understanding of the mechanism operating at the electrode surface was attained through EIS mea-

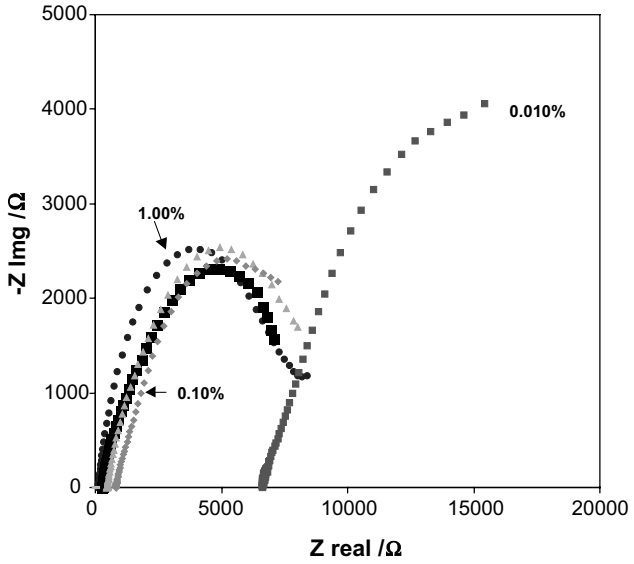

Fig. 5. Nyquist impedance diagrams as a function of Na_2SO_4 concentration.

surements at the corresponding corrosion potential, E_{corr}. All the impedance measurements were performed under potentiostatic conditions.

Impedance is a function of both frequency and the steady-state polarization condition. The interface impedance can be accurately measured frequency-by-frequency with a sinusoidal polarizing signal. At each frequency a digital transfer function analyzer (TFA) was used as first introduced by Gabrielli and Keddam [13].

All the impedance diagrams were validated by the Kramers–Kronig analysis [14].

The impedance diagrams obtained are characterized by capacitive behavior (Figure 5). From the Nyquist representation of the impedance for the percentages 1, 0.4, 0.2, 0.1 and 0.01%, it can be seen that as the Na_2SO_4 concentration decreases, the higher the high frequency limit of the impedance increases, since it is shifted to higher values on the Z_{real} axis (Figure 5).

An electrochemical system such as Fe/Na_2SO_4 can be considered as a simple corrosion process in which corrosion takes place uniformly. Vatankhah et al. [15], having studied the effect of sulfate ions on the electrochemical behavior of iron electrodes, point out that in solutions containing sulfate ions only, iron experiences uniform corrosion and sulfate ions are aggressive.

In some cases of outstanding theoretical relevance the faradaic impedance (Z_f) is frequency independent, being represented by a purely resistive component; the charge-transfer resistance (R_{ct}) is, therefore, equal to R_p. Such a situation is encountered in those cases in which the conditions of applicability of the polarization resistance technique are met: one-step, Tafelian, charge-transfer-controlled anodic and cathodic currents [16].

Considering a simple equivalent circuit in which the diffusional effects (Warburg impedance) are negligible (Figure 6), the expression describing a semicircle in the Nyquist representation is

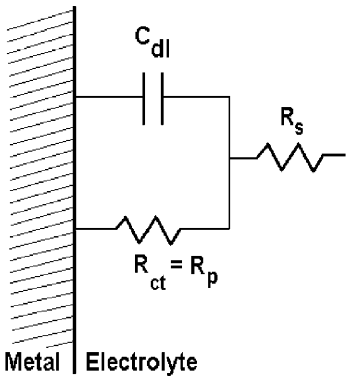

Fig. 6. Electrical equivalent circuit model for Fe/ Na_2SO_4 system.

$$\left(Z_r - R_s - \frac{R_{ct}}{2}\right)^2 + Z_i = \left(\frac{R_{ct}}{2}\right)^2 \tag{4}$$

with center (Z_r^*) on:

$$Z_r^* = R_s + \frac{R_{ct}}{2} \tag{5}$$

and radius, r:

$$r = \frac{R_{ct}}{2} \tag{6}$$

Then two events can be explained as follows: (a) from Equation 4, the center (Z_r^*) of each semicircle occurs at higher values on the Z_{real} axis and (b) from Equation 5 the radius (r) of each increases. By comparing the modulus of the measured impedance against frequency for the 1, 0.4, 0.2, 0.1, 0.01 and 0.001% Na_2SO_4 solutions, one can observe that as the Na_2SO_4 concentration decreases both the high (R_s) and low frequency limits increase.

The impedance response measured for the 0.001% Na_2SO_4 solution (related to the solution resistance) is in the same order of magnitude as R_{ct}, thus indicating a difficulty in trying to estimate R_p, that is, considering that $R_p = R_s + R_{ct}$, it is obvious that the measured response will be given mainly by R_s. For the 0.001% Na_2SO_4 solution a zero phase angle was measured (Figure 7b). This fact suggests that the potential and current are in-phase and, therefore, the measured response corresponds to that of a resistor that can be associated with the solution resistance (R_s). When the solution resistance is high, which occurs when the Na_2SO_4 concentration decreases, the effect of increasing R_s on the Bode plot is shown in Figures 7a and b.

The fitting of experimental results to the proposed equivalent circuit (shown in Figure 6) is very good, especially for Na_2SO_4 concentrations higher than 0.01%.

Figure 8 shows a quantitative comparison between the different techniques: LPR, EN and EIS. It is possible to note on this figure that the highest value for

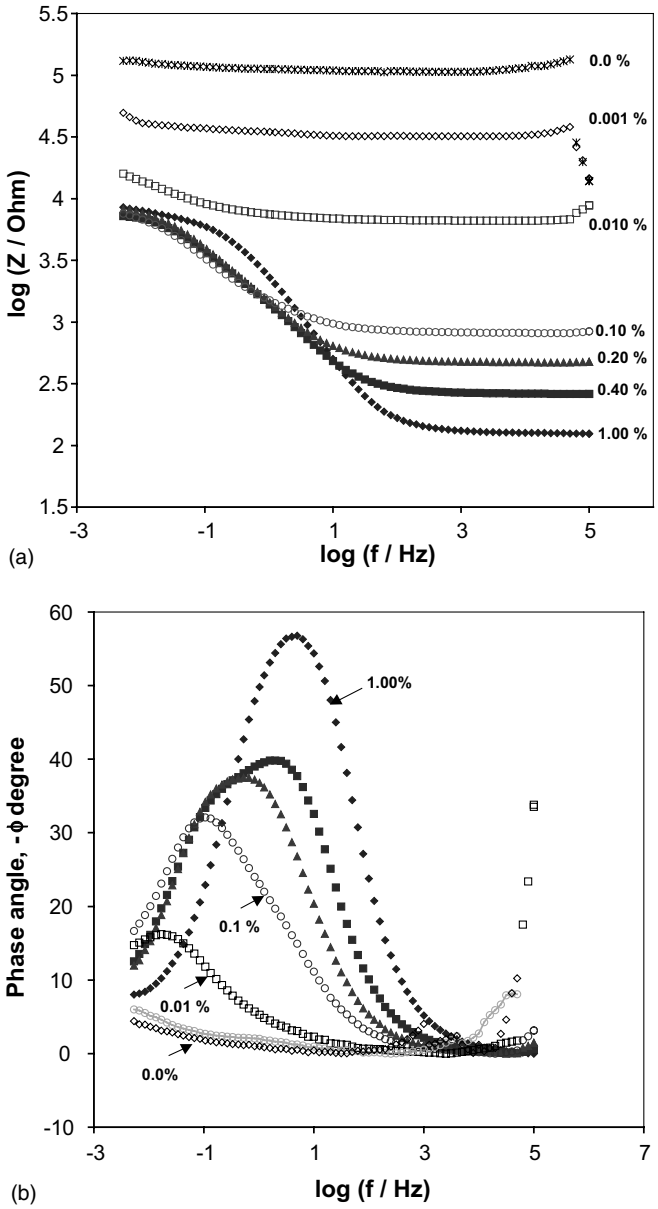

Fig. 7. (a) Bode plots (modulus) of AISI 1020 mild steel in aerated, neutral Na_2SO_4. Immersion time: 7 days. Effect of solution resistance on the Bode plot. (b) Bode plots (phase angle) of AISI 1020 mild steel in aerated, neutral Na_2SO_4. Immersion time: 7 days. Effect of solution resistance on the Bode plot.

the polarization resistance, R_p, was estimated by EN technique. Although three techniques had a similar trend they presented very different values. As Cottis [17] has pointed out comparison between EIS-R_p and R_n tend to ignore the difference in the effective frequency at which both variables are measured. Whereas R_p is typically measured at an effective frequency of $\sim 10^{-2}$ Hz (as in this case), R_n is normally measured using a range of frequencies up to ~ 1 Hz, consequently the two values may be quite different.

It has often been assumed that, because electrochemical noise measurements, ENM, do not involve the application of current to the cell, they are not susceptible to solution resistance effects. However, it appears that R_n incorporates the solution resistance in just the same way that R_p does [18]. Noise resistance can be easier to measure than LPR in solutions of high resistance, but the result is no more useful than R_p would be.

Mendoza-Flores [19] found a similarity between the calculated EN-R_s values and the calculated weight loss, WL, values. This fact suggests that when the R_s uncompensated EN values seems to be different to the WL values, they are actually similar, once a solution resistance compensation is taken into account.

Theoretically, the technique that better describes the corrosion phenomenon is weight loss because it represents the real corrosion conditions. However, in this work, we consider that the electrochemical technique better represent the corrosion of iron in Na_2SO_4 solutions as it takes into account the ohmic drop. For this reason EIS gives a good enough approximation to the real corrosion rates for the proposed system. The R_p

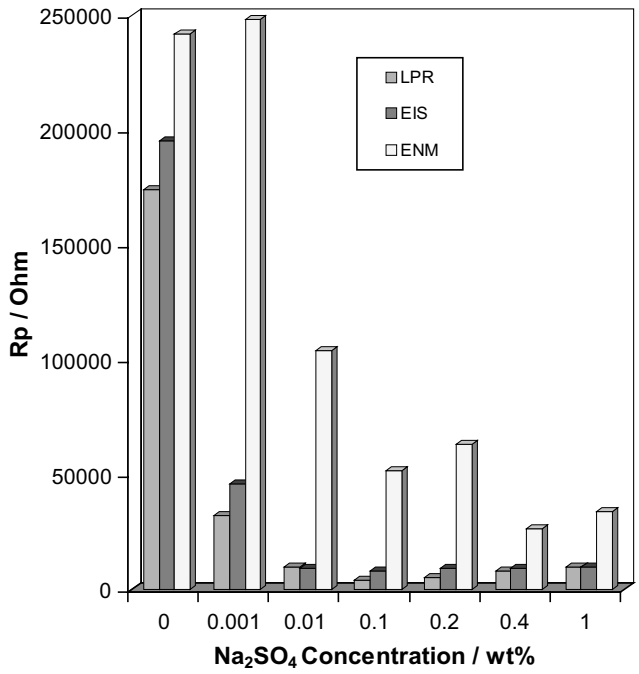

Fig. 8. Polarization resistance, R_p, determined by LPR, EIS and ENM as a function of Na_2SO_4 concentration.

values obtained from the LPR technique are significantly less than the values measured on the impedance diagram by extrapolation of the medium frequency semicircle, especially for the lowest concentrations. This may indicate that one or several time-constants exist in the low frequency range. The interface capacitance value calculated at the characteristic frequency of the semicircle ($C = 1/R_{ct}\omega$) is typical of a double layer capacitance value (40 μF cm^{-2}). This signifies that the medium frequency loop is related to a charge-transfer process, R_{ct} being the charge-transfer resistance.

The oxygen diffusion contribution is not seen on the diagram because it is likely to occur in the low frequency range. Under these conditions the R_{ct} value may be used as an indication of the corrosion rate of the system

$$R_{ct} = \frac{b_a b_c}{2.3(b_a + b_c)} \frac{1}{j_{corr}} = \frac{B}{j_{corr}}$$

The value for constant B calculated from anodic and cathodic Tafel slopes amount 26 mV which is very close to the value previously determined by Ohtsuka and Sato [20] of 25 mV.

4. Conclusions

Thermodynamically speaking, steel corrosion in Na_2SO_4 seems to occur by two different mechanisms:

For $<0.1\%$ Na_2SO_4 $\quad Fe_{(s)} \Leftrightarrow Fe^{2+}{}_{(aq)} + 2e$

For $\geqslant 0.1\%$ Na_2SO_4 $\quad SO^{2-}_{4(aq)} + Fe_{(s)} \Leftrightarrow FeSO_{4(aq)} + 2e$

In accord with the proposed mechanism, the corrosion rate of AISI 1020 mild steel increases significantly above 0.1% Na_2SO_4.

EIS diagrams do not give relevant information concerning the proposed mechanism. The impedance diagrams obtained show a capacitive semicircle, which is characteristic of a charge-transfer process, especially for the higher concentrations studied, its behavior being only resistive for the lower. R_p values determined from EIS follow a behavior similar to that obtained by LPR and ENM, showing a significant decrease under 0.001% Na_2SO_4.

Acknowledgements

This work was financed by CONACYT (Project 0726P-A9506) and by UAM-Azcapotzalco, DCBI (Project 2260220). S. Arzola is grateful for the grant given by CONACYT for his postgraduate studies.

References

1. G.H. Booth, A.W. Cooper and P.M. Cooper, *Br. Corr. J.* **2** (1967) 109.
2. UNDA Handbook, No. 60, L.A. Richard (Ed.), (US Department of Agriculture, Washington, DC, 1969).
3. A.W. Peabody, 'Control of Pipeline Corrosion', *in* R.L. Bianchetti (Ed.), 2nd edn. (NACE International, Houston, 2001) p. 90.
4. M. Romanoff, Underground Corrosion, Circular 579 (National Bureau of Standards US, 1957).
5. A. Rojas-Hernández, M.T. Ramirez, J.G. Ibañez and I. Gonzalez, *J. Electrochem. Soc.* **138** (1991) 365.
6. J.G.N. Thomas, A.D. Mercer and J.D. Davies, *in* R.H. Heusler (Ed.), Proceedings of the International Conference on Corrosion Inhibition, (1983), p. 89.
7. J. Gui and T.M. Devine, *Corros. Sci.* **37** (1995) 1177.
8. B.G. Pound, G.A. Wright and R.M. Sharp, *Corrosion* **45** (1989) 386.
9. G.M. Florianovitch, L.A. Sokolova and Ya.M. Kolotyrkin, *Electrochim. Acta* **12** (1967) 879.
10. S. Szklarska-Smialowska and G. Mrowczynski, *Br. Corr. J.* **10** (1975) 187.
11. J.M. Abd El Kader, A.A. El Warraky and A.M. Abd El Aziz, *Br. Corr. J.* **33** (1998) 145.
12. D.M. Brasher, *Nature* **193** (1962) 868.
13. C. Gabrielli and M. Keddam, *Electrochim. Acta* **19** (1974) 355.
14. M. Urquidi-MacDonald and D.D. MacDonald, Software Kramers–Kronig (Penn State University, 1999).
15. G. Vatankhah, M. Drogowska and H. Menard, *J. Appl. Electrochem.* 28 (1998) 173.
16. I. Epelboin, C. Gabrielli, M. Keddam and H. Takenouti, Alternating-current impedance measurements applied to corrosion studies and corrosion-rate determination, *in* F. Mansfeld and U. Bertocci (Eds), 'Electrochemical Corrosion Testing', ASTM STP 727 (American Society for Testing Materials, Philadelphia, 1981) pp. 150–166.
17. R.A. Cottis, *Corrosion* **57** (2001) 265.
18. R.A. Cottis and S. Turgoose, *in* Barry C. Syrett (Ed.), 'Electrochemical Impedance and Noise', (NACE International, Houston, 1999) p. 77.
19. J. Mendoza-Flores, MSc Thesis, Institute of Science and Technology, University of Manchester, Manchester, (1993).

20. T. Ohtsuka and N. Sato, *Corros. Eng.* **31** (1982) 336.
21. A. Rojas and I. González, *Anal. Chim. Acta* **187** (1986) 279.
22. A. Rojas-Hernández, M.T. Ramírez, I. González and J.G. Ibáñez, *Anal. Chim. Acta* **259** (1992) 95.
23. Ibid., *Anal. Chim. Acta* **278** (1993) 321.
24. Ibid., *Anal. Chim. Acta* **278** (1993) 335.
25. Ibid., *J. Chem. Ed.* **72** (1995) 1099.
26. G. Sillén, Stability Constants of Metal-Ion Complexes, Special Pub. No. 17 (The Chemical Society, London, 1971).
27. R.M. Smith and A.E. Martell, 'Critical Stability Constants', Vol. 2 and 4 (Plenum Press, New York, 1975).
28. E. Högfeldt, 'Stability Constants of Metal–Ion Complexes: Part A-Inorganic Ligands', IUPAC Chemical Data Series, No 21 (Pergamon Press, Inc., New York, 1979).

Appendix 1

PZD construction for the Fe(II)–H_2O–SO_4^{2-} system

Rojas et al. [5, 21–25] have proposed a method for the construction of two dimensional PZD for non-redox chemical species, with interpretations and applications similar to those of Pourbaix diagrams. We have followed this theory for the construction of Figure 1. In order to simplify the calculations, we have used the concepts of 'donor', 'acceptor', 'particle', 'conditional constants', 'generalized species' and 'representative equilibrium'. The chemical species considered here, and the equilibrium constants that regulate the relationships among them come from various sources [26–28]. Table A.1 summarizes the data used to construct the diagram of the Fe(II)–H_2O–H^+–SO_4^{2-} system.

For the chemical interaction between the species Fe(II) and OH^-, different equilibriums were considered, i.e:

Successive formation

$$Fe^{2+} + OH^- \Leftrightarrow FeOH^+ \quad (A.1)$$

$$FeOH^+ + OH^- \Leftrightarrow Fe(OH)_2 \quad (A.2)$$

$$Fe(OH)_2 + OH^- \Leftrightarrow Fe(OH)_3^- \quad (A.3)$$

$$Fe(OH)_3^- + OH^- \Leftrightarrow Fe(OH)_4^{2-} \quad (A.4)$$

Table A.1. Data used to construct the diagram of the Fe(II)–H_2O–H^+–SO_4^{2-} system

Equilibrium	log *K*
$Fe^{2+} + OH^- \Leftrightarrow FeOH^+$	4.50
$Fe^{2+} + 2OH^- \Leftrightarrow Fe(OH)_2$	7.40
$Fe^{2+} + 3OH^- \Leftrightarrow Fe(OH)_3^-$	10.00
$Fe^{2+} + 4OH^- \Leftrightarrow Fe(OH)_4^{2-}$	9.60
$Fe^{2+} + SO_4^{2-} \Leftrightarrow FeSO_4$	2.20
$Fe^{2+} + HSO_4^- \Leftrightarrow FeSO_4 + H^+$	0.19
$HSO_4^- \Leftrightarrow SO_4^{2-} + H^+$	−2.01
$H_2O \Leftrightarrow OH^- + H^+$	−14.00

Global formation

$$Fe(OH)_2 + 2OH^- \Leftrightarrow Fe(OH)_4^{2-} \quad (A.5)$$

And those related to the possible dismutation of the system's ampholytes:

$$2Fe(OH)_3^- \Leftrightarrow Fe(OH)_4^{2-} + Fe(OH)_2 \quad (A.6)$$

To illustrate the notation used, the thermodynamic equilibrium constant for reaction (A.1) above is written:

$$K_{FeOH^+}^{Fe^{2+},OH^-} = \frac{[FeOH^+]}{[Fe^{2+}][OH^-]}$$

and the constant for reaction (A.2) is written in terms of analogous constants for the first two reactions shown in Table A.1.

$$K_{Fe(OH)_2}^{FeOH^+,OH^-} = \frac{K_{Fe(OH)_2}^{Fe^{2+},2OH^-}}{K_{FeOH^+}^{Fe^{2+},OH^-}}$$

Other reactions and constants are treated analogously. It has been shown [21] that for any M and L species, if $K_{ML_2,M}^{2ML} < 1$ (or $K_{ML}^{M,L} > K_{ML_2}^{ML,L}$) the PZD is

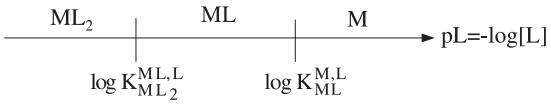

whereas if $K_{ML_2,M}^{2ML} \geq 1$, the PZD is

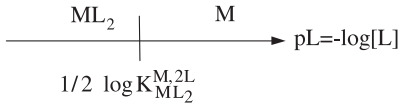

In the case analyzed here, for the soluble iron(II) hydroxo complexes, we found:

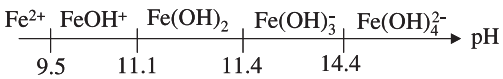

and for the iron(II) sulfate complexes:

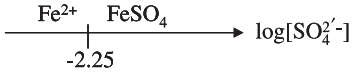

A two-dimensional PZD ($pSO_4^{2'-}$ vs pH) for the soluble species of Fe(II) can summarize the effects that buffering with $SO_4^{2'-}$ or changes in pH produce on the system. In this case, $SO_4^{2'-}$ is the first-order generalized species defined by

$$SO_4^{2'-} = HSO_4^- + SO_4^{2'-}$$

By means of the two one-dimensional diagrams of iron complexes, we found that the $pSO_4^{2'-}$ vs. pH diagram can be constructed using the representative equilibria shown in Table A.2:

With these last equilibria it is possible to construct Figure 1. The establishment of conditions under which a given species may predominate in the system has practical significance because the physicochemical properties of the system depend on the relative importance of this species.

Table A.2. Data used to construct the $pSO_4^{2\prime-}$ vs pH diagram

If	Representative equilibrium	$pSO_4^{2\prime-}$
$pH \leqslant 2.012$	$Fe^{2+} + HSO_4^- \Leftrightarrow FeSO_4 + H^+$	$0.188 + pH$
$2.012 \leqslant pH \leqslant 9.5$	$Fe^{2+} + SO_4^{2-} \Leftrightarrow FeSO_4$	2.2
$9.5 \leqslant pH \leqslant 11.1$	$FeOH^+ + SO_4^{2-} + H^+ \Leftrightarrow FeSO_4 + H_2O$	$11.7 - pH$
$11.1 \leqslant pH \leqslant 11.4$	$Fe(OH)_2 + SO_4^{2-} + 2H^+ \Leftrightarrow FeSO_4 + 2H_2O$	$22.8 - 2pH$
$pH \geqslant 11.4$	$Fe(OH)_3^- + SO_4^{2-} + 3H^+ \Leftrightarrow FeSO_4 + 3H_2O$	$34.2 - 3pH$